Physics Journal
Vol. 4, No. 1, 2018, pp. 1-8
http://www.aiscience.org/journal/pj
ISSN: 2471-8483 (Print); ISSN: 2471-8491 (Online)

Characterization of Point–Plane Corona Discharge in Oxygen with Monte Carlo Method

A. Settaouti*

Electrotechnic Department, University of Sciences and Technology, Oran, Algeria

Abstract

The corona discharge commonly occurs in many processes and engineering devices. Monte Carlo simulation for the initial phase of an oxygen corona discharge in apoint-plane gap is presented. This method is based on the motion of electrons in electric field and their interactions with the molecules of gas. All the electrons are followed simultaneously in time and their coordinates and velocities are recorded. It lets us study all space and temporal aspects of the electron avalanche evolution. The growth of the first avalanche and the beginning of the second one are simulated to determine which physical process is responsible for the propagation of the discharge. This method provides the spatial-temporal local electric field and particles charged densities variations as well as the ionization front velocity.

Keywords

Simulation, Monte Carlo, Corona, Electric Field, Space Charges, Discharge

Received: July 29, 2015 / Accepted: August 12 / Published online: March 24, 2018

1. Introduction

Corona discharges have attracted much attention in recent years due to their broad applications, and have potential applications in biomedical and surface treatment, chemical and biological decontamination, aerodynamic flow control, and combustion [1-5]. Corona discharges are being actively studied in connection with their plasma chemical applications, such as removal of toxic agents from flue gases and from polluted air [6-8]. The dc corona with spraying discharge electrodes was employed in electrostatic pesticide spraying successfully [9, 10]. Corona discharges are industrially employed to treat large areas of polymer; most processes use the discharges to affix oxygen to hydrocarbon polymers, thereby increasing their surface energy and wettability. This high voltage corona discharge method is used for rendering the surfaces more receptive to adhesives and decorative coatings by creating new surface functional groups. The corona discharge oxidizes the surface making this surface receptive to coatings; another processing function of corona discharge is the poling of polymers and ferroelectric materials [11]. In recent years, electronegative gases have become important in technologies that use discharges for processes such as etching and plasma discharge deposition on substrates.

The corona discharge has been a main concern for power transmission, corona discharges are undesirable on the power transmission lines because of their power loss and induction effect on ground objects. Also, the corona discharges produce electromagnetic interferences on communication antennas and audible noise [12-15]. All of this reflects on the great importance of the evaluation of the corona discharge characteristics.

The corona discharge is a dynamic process; all parameters vary in time if a voltage is applied. In many cases the numerical simulation of the corona discharge is necessary for predicting the performance of a device [16-19]. The simulation of electric fields is crucial in the design process of

* Corresponding author
E-mail address: Settaouti@yahoo.fr

insulation parts in electric devices. A simulation, which could predict these distributions for given voltage, electrode geometry and parameters of the ambient gas are very useful in practical applications. In the work presented here we examine the negative corona discharge in oxygen in order to arrive at a better understanding of its mechanism. We use the Monte Carlo method to calculate the behavior of the corona discharge.

2. The Numerical Model

The physical model of the corona discharge is rather complicated; the growths of electronic avalanches are modelled using Monte Carlo method. Monte Carlo simulations model these effects contain the full microscopic physics; the electron motion between collisions is calculated and collisions of electrons with neutrals are treated with appropriate statistical weights. The simulation also included the release of electron ion pairs by photoionization [20, 21], new electrons, positive and negative ions may be produced by ionization, photoionization and attachment collisions. Due to the influence of the non-uniform electric fields on the real probability of each analyzed collision process, the Monte Carlo method take into account the phenomena of non-equilibrium electron kinetics, and the incorporating the effects of the distortion due to the space charge on the applied electric field. The initial electrons are emitted from the cathode according to a cosine distribution for the entry angles. Whether a collision between an electron and a gas molecule occurs or not is decided by generating a random number R_1 uniformly distributed between 0 and 1. Collision is assumed to have occurred at the end of a time step if the condition $P \geq R_1$ is satisfied, where P is the probability of collision. If the random number is larger than P, no collision has occurred and the particle follows its way as if nothing has happened. The probability of collision over the time step Δt is

$$P = \left[1 - \exp\left(\frac{-\Delta t}{t_m}\right)\right] \tag{1}$$

$$t_m = \frac{1}{N.Q_t(\varepsilon).v(\varepsilon)} \tag{2}$$

in which $v(\varepsilon)$ is the velocity of an electron, Q_t the total collision cross section, N the gas number density, ε the electron energy and t_m is the electron means collision time. When a collision occurs between an electron and a gas molecule, the type of collision is determined by generating a random number R_2, this too being uniformly weighted between 0 and 1. The segment into which R_2 falls determines the type of collision that has occurred [19, 22]. Where no new particles are produced the electron loses the energy corresponding to the type of collision. However, in the case of an ionizing collision, after subtracting the threshold energy, the remaining energy is evenly ascribed to the two electrons. To determine the nature of the collision, the total collision cross section Q_t is split up into its component collision cross sections for all possible collision processes of the electron, and the fractional probability of a certain kind of collision is computed.

$$P_{2,j} = \frac{Q_j}{Q_t} \quad \sum P_{2,j} = 1 \tag{3}$$

Where $P_{2,j}$ are the fractional probability of a attachment, ionization, excitation, rotational, vibration and elastic collision for an electron. At a given electron energy ε, the sum of the fractional probabilities is equal to unity and the interval [0, 1] is divided into segments of lengths corresponding to these fractional probabilities. A random number (R_2) between 0 and 1 is generated and the segment into which this random number falls, determines the type of collision that has occurred. The nature of the collision is determined in the following way: $P_{2,j}$ is the probability that collision process j (the elastic, attachment, vibration, rotational, excitation and the ionization collisions) takes place, j = 1, 2, 3,..., n:

$$P_{2,1} + P_{2,2} + \ldots P_{2,j-1} < R_2 \leq P_{2,1} + P_{2,2} + \ldots P_{2,j} \tag{4}$$

This leads to determine the jth type of collision. After the collision, the particle follows its way during the next time step and procedure is repeated. The temporal development of electron and ion populations in a point-plane gap is calculated in the simulation by simultaneously following the trajectories of a large number of individual electrons. The development of the electron avalanche is assumed to occur along the axis of the gap. The model is one dimensional in position space and three dimensional in velocity space. In the simulation of a corona discharge, the time step and the cell size should receive much attention. For any shape or type of ionizing electrode, the corona discharge is characterized by two regions: a thin layer, very close to the active electrode surface called ionization zone, and a drift zone toward a collecting electrode. This study is performed in a point-plane gap, note that it is necessary to follow the region where the electric field changes most rapidly, with a fine mesh. For the purpose of simulation, the gap between a point electrode and a plane is divided into two regions: regions 1 close to the point electrode where the electric field is high and most electrons and ions are located, and region 2 the rest of the gap. In region 1, electron motion is simulated by dividing the region into a number of cells; a small cell size improves the accuracy. Also the accumulation of space charge causes the

electric field in region 1 to change abruptly over space, and therefore a smaller cell size Δz_1 is used. In contrast, in region 2, a larger cell size Δz_2 is adequate. The length of region 1 may vary with various voltages and gap separations.

$$\Delta z_1 = \frac{d_1}{M_1}, \ \Delta z_2 = \frac{d - d_1}{M_2} \tag{5}$$

Where M_1 and M_2 are the cell numbers in region 1 and region 2, respectively, d is the gap length and d_1 is the length of region 1. In a simulation of corona discharge based on the Monte Carlo method, the electrons and ions, if exceeding a certain number, distort the electric field and all the electrons are followed over the same time interval. When all electrons have been followed, we move to the next time step to follow all the electrons again, i.e., the electrons are stored after being followed during the previous time step, and new electrons are created by ionization collisions during the previous time step. The time interval should be small, and less than the mean flight time. At the end of each time step, the space charge field is calculated from the Poisson's equation as a function of charge distribution and is stored for use over the next time step, the total electric field is the sum of the Laplacian field and the space charge field [19, 22]. It is noted that the principal advantage of the Monte Carlo method lies in the fact that swarm parameters are not required for the simulation.

3. Results and Discussion

We use the Monte Carlo method for the simulation of the corona discharge; it lets us study all temporal and space aspects of the electron avalanche development. Corona discharges, in general, are generated in electrode systems characterized by high non-uniformity of electric field. Results are obtained for a negative corona discharge in O_2 in a point - plane geometry. The calculations are performed at a gas number density $N=2.12\times10^{24}$ m^{-3} at 3 kV. The cross section set of O_2 employed is that referred in [23]. The axial electric field distribution at any point along the axis of the gap is approximated as [24, 25]

$$E(z) = \frac{2V_0}{\ln\left(\frac{4d}{r_1}\right)} \cdot \frac{1}{2z + r_1 - z^2/d} \tag{6}$$

where r_1, d, z and V_0 are respectively the tip radius, gap length, distance from the point electrode and applied voltage. For the purpose of simulation, the gap between the point and the plane is divided into two regions, the gap parameters are $d = 5\times10^{-3}$ m, $r_1 = 5\times10^{-4}$ m, $d_1 = 1\times10^{-3}$ m, $M_1 = 50$ and $M_2 = 100$. According to the calculation of mean flight times, the time step 0.5×10^{-12} s is chosen in this study.

The simulation starts from a given number of electrons deposited at the cathode, these electrons are then simultaneously traced in the electric field in given time steps. The initiation and development of successive avalanches are traced as a function of time after voltage is applied. The simulation provides a detailed structure of avalanches from which the total electric field distribution and propagation of successive avalanches can be discerned. The development of electron avalanches are due to ionization and photo-ionization and quenching of avalanches is due to the low electric field. Without the photoionization process near or at the cathode, the electron may multiply into an avalanche through ionization processes, all electrons will eventually travel to the anode and the discharge will be extinguished. The photoionization position is determined by comparing the probability of the photoionization point, which is proportional to the solid angle extended from the excitation point to the plane contained photoionization point, with computer generated random numbers at the end of each step, when one ion - electron pair is produced due to photoionization. Then, an ion electron pair is stored, with 0.1 eV energy for the electron generated by photoionization.

The electric field plays a key role in corona discharge development, in order to understand the physical process; the evolution of several electric field profiles in the gap is shown in Figures 1-2. Due to the large differences in the mobilities of electrons and ions, the ions are considered to be relatively stationary; this causes a distortion of the total electric field. From Figure 1, it is clear that up to 1.1 ns, there is a negligible distortion of the total electric field from the Laplacian field. The ions, almost stationary in the time scale of motion of the electron avalanche, remains behind. The space charge distortions in these situations are sufficiently significant to perturb the applied electric field. Later, the space charge enhances the electric field at both sides of the electron avalanche and weakens the electric field in avalanche space (Figure 1 and Figure 2). A plasma region is formed close to the cathode, as the high ionized region grows; the region with a high electric field at the cathode becomes narrow. We can also see the electric field intensity becomes stronger gradually with time between point electrode and positive ions, due to the space charge effect. The negative sign of the total electric field means the space charge field exceeds the applied electric field at the same position, but with a reversed direction. This is due that the ionization processes in the high electric field region cause more positive ions in a small region, the space charge field is very high, even higher than the applied electric field.

The initiation and development of successive avalanches of electrons are traced as a function of time (Figures 3-4). When the initial electrons are emitted from the cathode, the primary

avalanche drifts toward the anode and multiply fast to 0.5 ns. While the primary avalanche builds up toward anode, excitation of atoms has been taking place at the same time ionization events have been occurring. Thus, before the primary avalanche has reached its full size, photons will be emitted from these excited states as they return to the ground state. These photons will be emitted in all directions and will be absorbed at various distances from their origin, new electrons and positive ions may be produced by photoionization.

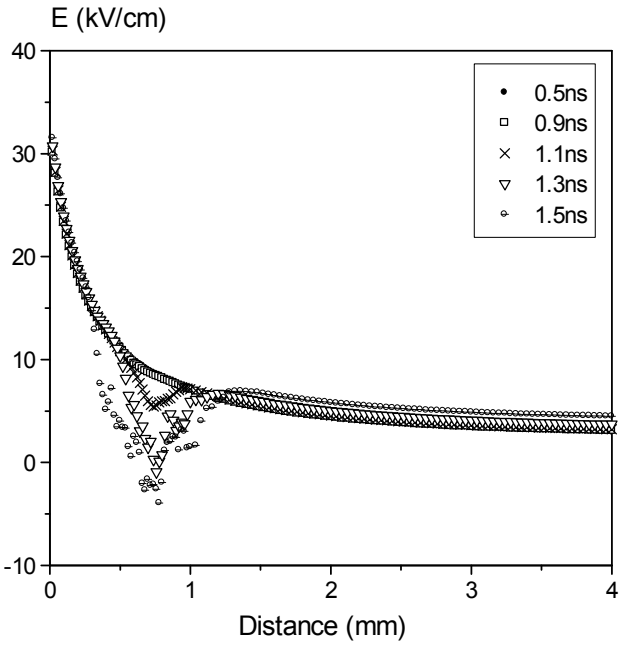

Figure 1. E (kV/cm) as a function of distance.

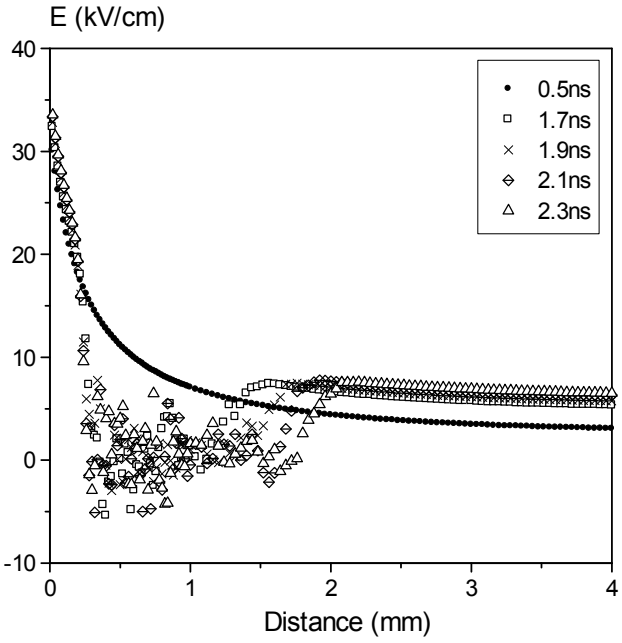

Figure 2. E (kV/cm) as a function of distance.

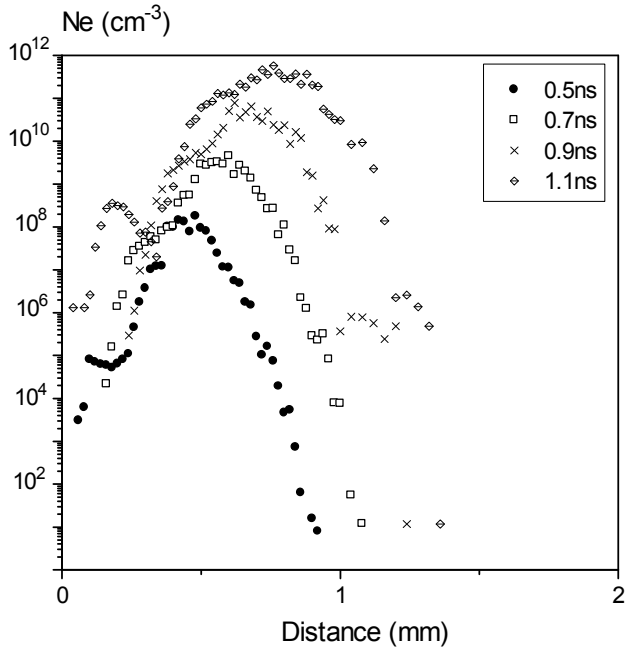

Figure 3. Electron density as a function of distance.

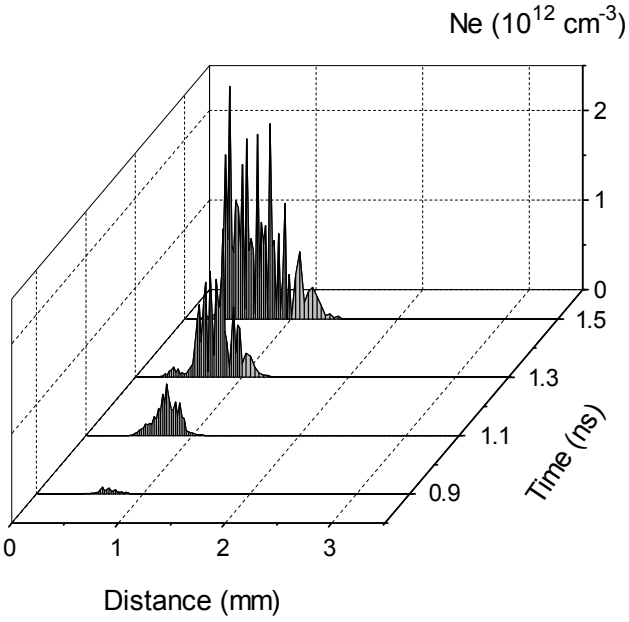

Figure 4. Temporal-spatial variations of electron density.

At the time 0.5 ns, a second avalanche is initiated by photoionization and grows faster than the primary avalanche because it is in the high electric field region close to cathode. It should be noted that the photoionisation can occur in an area of low electric field, but the avalanche will extinguish quickly because oxygen is an electronegative gas. Only the avalanches started in a high electric field region will develop. With the availability of the photoelectrons in oxygen, successive avalanches of second generations are generated at various distances from the primary avalanche. Like for the

development of the primary avalanche, all the successive avalanches of second generation will emit photons after their formation. These photons create new photoelectrons which will start a third generation of avalanches and so on.

At t = 1.1 ns, a third avalanche is initiated in the high electric field region. The second avalanche decays as time increases, the third avalanche grows and begins to decrease (Figure 4) later because the total electric field in its region decreases. The second and third avalanches continue to decline, and then appears a fourth avalanche close to the cathode. The electric field distortion increases with time, the positive space charge close to the electrode increases the incline of the electric field, enhancing the electric field at the cathode surface. The electric field further from the cathode is reduced almost to zero; the electric field has a steep gradient near the ionization front where the ionization is proceeding (Figure 5).

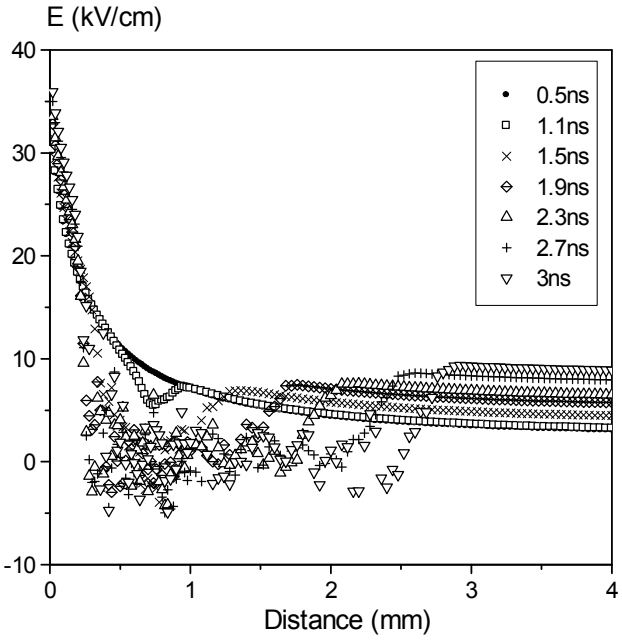

Figure 5. E (kV/cm) as a function of distance.

As the charge densities increase, space charge effects decrease the electric field near the point electrode. With the displacement of the high density area towards cathode, a denser space charge develops close to cathode, which leads to an enhancement of the electric field on the cathode side and reduce it in the space charge. The enhancement of the electric field adds to an already high Laplacian field towards the point electrode, results in enhanced ionization in this region, causing the increase of electrons and positive ion densities towards the cathode side.

Due to reduction of the electric field within the space charge, the ionizations are reduced while the attachments increase. Elastic collisions of the electron with background gas molecules slow down the electron's motion toward the anode and randomize the directed kinetic energy along the electric field in all three directions. The position of the densities peaks of the electron and positive ion remain nearly stationary. The charged particles density profiles (Figures 6-11) extend to the plane electrode, and their peak values decrease gradually, this effect is due to the decreases in the electric field.

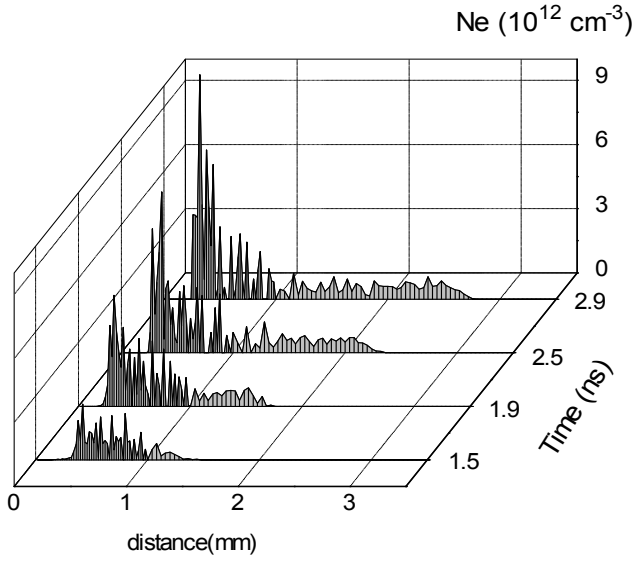

Figure 6. Temporal-spatial variations of electron density.

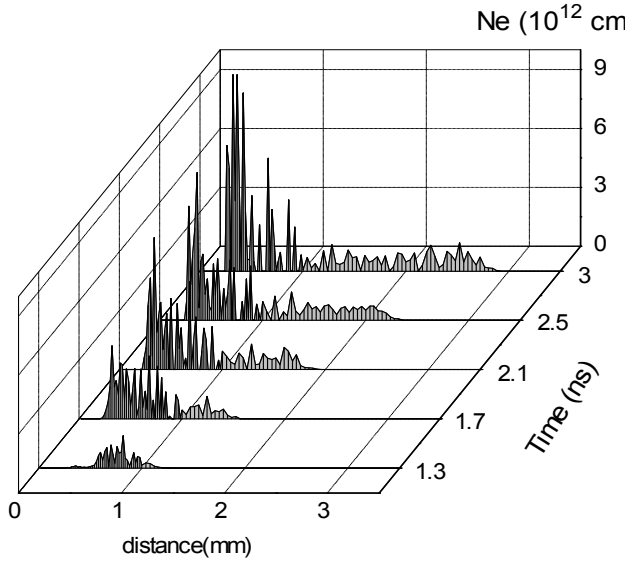

Figure 7. Temporal-spatial variations of electron density.

The combined effect of enhanced ionization in the region between cathode and the space charge, with reduced ionization along space charge, increased attachment in space charge region, leads to the shifting of the electron and ion

density peaks, hence the space charge shifts towards the cathode. When the electrons are in the low electric field region and finally attach to molecules and decrease with time, there is only a narrow high electric field region close to cathode usually called the cathode fall region. The peaks of the positive ions distributions decrease and moves toward the cathode, because at later stages ionization can occur only in the high electric field region (Figures 8-10).

The negative ion distributions are similar to those of positive ions with a slightly smaller peak (Figure 11). The net charge also depends on electron density, which changes rapidly with time, the net charge distributions do not stabilize. A large positive peak always seems to be followed by a negative peak (Figure 12).

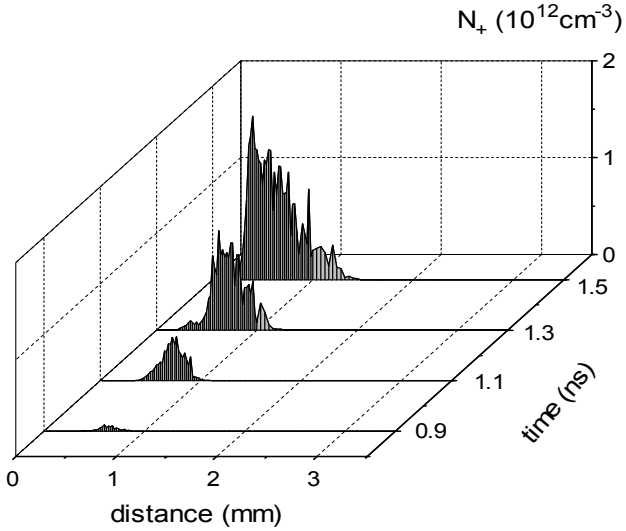

Figure 8. Temporal-spatial variations of positive ion density.

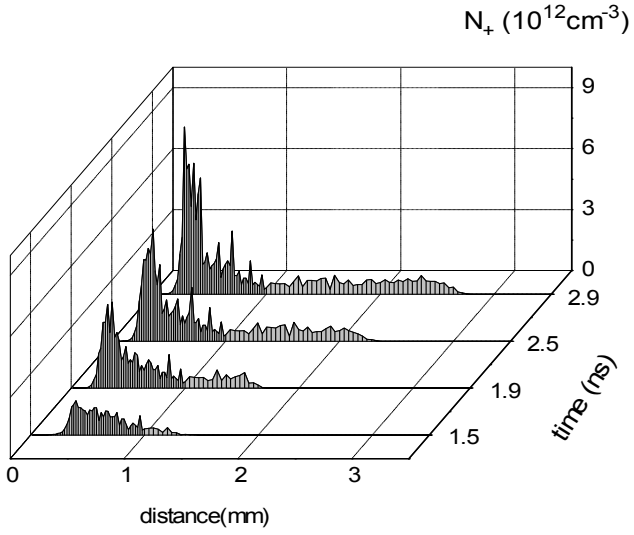

Figure 9. Temporal-spatial variations of positive ion density.

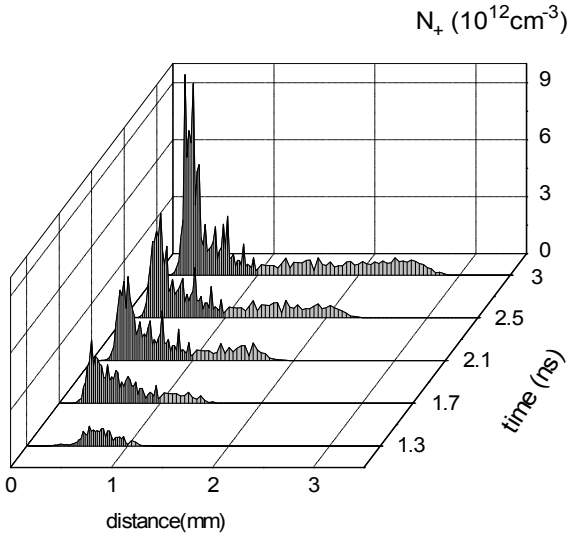

Figure 10. Temporal-spatial variations of positive ion density.

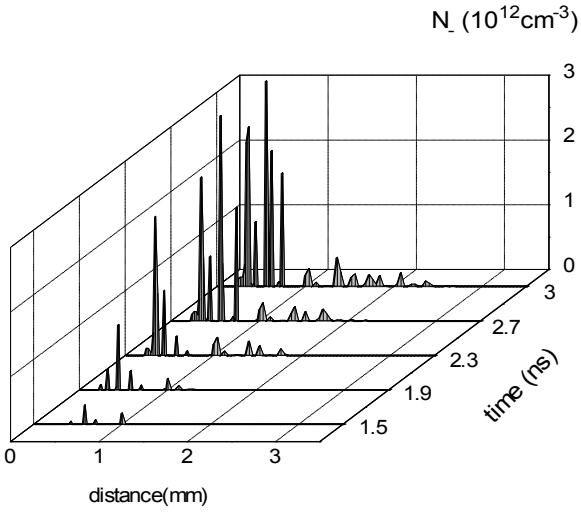

Figure 11. Temporal-spatial variations of negative ion density distribution.

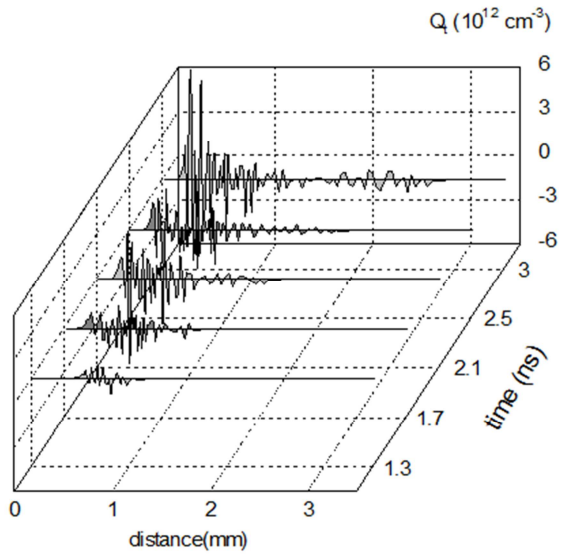

Figure 12. Temporal-spatial variations of the net charge density.

The densities of charged species inside the avalanche body near the point are on the order of 10^{13} cm^{-3}, which agrees with the results reported in Refs. [26-28]. The result of the propagation velocity of the ionization front is about 4.6×10^{7} cm/s.

The calculated values for the frontal velocities agree well with the experimental results [29-32] and with those reported in Refs. [26, 28, 33-35]. Measurements [29, 30] of the average propagation velocity of the ionization front extend from 2×10^{7} to 5×10^{7} cm/s, the propagation average velocity [33, 34] of the ionization wave is approximately of 5×10^{7} cm/s, these results are in good agreement with our calculated data.

The simulation provides a detailed structure of avalanches, and the propagation of successive avalanches.

4. Conclusion

The calculation describing the dynamical behavior of the corona discharge in oxygen was studied. The spatial-temporal local electric field, charged particles densities variations and the velocity profile of the ionizing front are obtained by using a Monte Carlo method. The advantage of the Monte Carlo method lies in the fact that swarm parameters are not required for the simulation. The simulation provides a detailed structure of avalanches, and propagation of successive avalanches can be discerned. The results show that space charge effects by positive ions swarms intensify the electric field between cathode and positive ions so that the discharge in this region becomes more stable. At the same time they decrease the electric field between positive ion swarm and anode so that the corona discharge expansion toward anode is restrained with time. From these results, the space charges and the photoionization play an important role in the progress of the corona discharge.

References

[1] A. A. Martins, M. J. Pinheiro, "Modeling of an EHD corona flow in nitrogen gas using an asymmetric capacitor for propulsion", J. Electrostatics 69 (2011) 133-138.

[2] E. Moreau, N. Benard, J. D. Lan-Sun-Luk, J. P. Chabriat, "Electrohydrodynamic force produced by a wire-to-cylinder dc corona discharge in air at atmospheric pressure", J. Phys. D: Appl. Phys. 46 (2013) 475204.

[3] PhBéquin, V. Joly, Ph Herzog, "Modeling of a corona discharge microphone", J. Phys. D: Appl. Phys. 46 (2013) 175204.

[4] C. Lee, J. Kim, J. Yoon, "Inactivation of MS2 bacteriophage by streamer corona discharge in water", Chemosphere 82 (2011) 1135-1140.

[5] R. Bussiahn, R. Brandenburg, T. Gerling, E. Kindel, H. Lange, N. Lembke, K. D. Weltmann, Th. von Woedtke, T. Kocher, "The hairline plasma: An intermittent negative dc-corona discharge at atmospheric pressure for plasma medical applications", Appl. Phys. Lett., 96 (2010) 143701.

[6] M. Sato, "Environmental and biotechnological applications of high-voltage pulsed discharges in water", Plasma Sources Sci. Technol., 17 (2008) 024021.

[7] G. J. J. Winands, K. Yan, A. J. M. Pemen, S. A. Nair, Z. Liu, E. J. M. van Heesch, "An industrial streamer corona plasma system for gas cleaning", IEEE Trans. Plasma Sci., 34 (2006) 2426-2433.

[8] L. Lei, Y. Zhang, X. Zhang, Y. Shen, "Using a novel pulsed high-voltage gas–liquid hybrid discharge, continuous reactor for removal of organic pollutant in oxygen atmosphere", J. Electrostatics 66 (2008) 16-24.

[9] N. Shirai, R. Sekine, S. Uchida, F. Tochikubo, "Atmospheric negative corona discharge using Taylor cone as a liquid cathode", Jpn. J. Appl. Phys., 53 (2014) 026001.

[10] S. N. Abolmasov, L. Kroely, P. Roca i Cabarrocas, "Negative corona discharge: application to nanoparticle detection in rf reactors", Plasma Sources Sci. Technol. 18 (2009) 015005.

[11] A. N Bhoj, M. J Kushner, "Continuous processing of polymers in repetitively pulsed atmospheric pressure discharges with moving surfaces and gas flow", J. Phys. D: Appl. Phys. 40 (2007) 6953-6968.

[12] U. Straumann, "Mechanism of the tonal emission from ac high voltage overhead transmission lines", J. Phys. D: Appl. Phys. 44 (2011) 075501.

[13] M. Becerra, "Glow corona generation and streamer inception at the tip of grounded objects during thunderstorms: revisited", J. Phys. D: Appl. Phys. 46 (2013) 135205.

[14] J. C. Matthews, J. P. Ward, P. A. Keitch, D. L. Henshaw, "Corona ion induced atmospheric potential gradient perturbations near high voltage power lines", Atmospheric Environment 44 (2010) 5093-5100.

[15] J. C. Matthews, A. J. Buckley, P. A. Keitch, M. D. Wright, D. L. Henshaw, "Measurements of corona ion induced atmospheric electricity modification near to HV power lines", J. Phys.: Conf. Series 142 (2008) 012044.

[16] U. Straumann, "Simulation of the space charge near coronating conductors of ac overhead transmission lines", J. Phys. D: Appl. Phys. 44 (2011) 075502.

[17] P. Wang, F. Fan, F. Zirilli, J. Chen, "A Hybrid Model to Predict Electron and Ion Distributions in Entire Interelectrode Space of a Negative Corona Discharge", IEEE Trans. Plasma Sci., 40 (2012) 421-428.

[18] R. Tirumala, D. B. Go, "Comparative study of corona discharge simulation techniques for electrode configurations inducing non-uniform electric fields", J. Electrostatics 72 (2014) 99-106.

[19] A. Settaouti, L. Settaouti, "Numerical simulation of streamer propagation in oxygen", Int. J. Modern Phys. B. 22 (2008) 293-307.

[20] G. W. Penney, G. T. Hummer, "Photoionization measurements in air, oxygen and nitrogen", J. Appl. Phys. 41 (1970) 572-577.

[21] M. Aints, K. Kudu, A. Haljaste, T. Plank, "Origin of photoionizing radiation in corona discharges in air", J. Phys. D: Appl. Phys. 34 (2001) 905-908.

[22] A. Settaouti, "Monte Carlo simulation of avalanche formation and streamer discharge", Electr. Eng., 92 (2010) 35-42.

[23] S. Kajita, S. Ushirata, Y. Kondo, "Influence of the dissociation process of the electron swarm parameters in oxygen", J. Appl. Phys., 67 (1990) 4015-4023.

[24] B. Florkowska, R. Wlodek, "Pulse height analysis of partial discharges in air", IEEE Trans. Electr. Insul. 28 (1993) 932-940.

[25] K. Adamiak, V. Atrazhev, P. Atten, "Corona discharge in the hyperbolic point-plane configuration: direct ionization criterion versus approximate formulations", IEEE Trans. Dielectr. Electr. Insul. 12 (2005) 1025-1034.

[26] E. Moreau, "Airflow control by non-thermal plasma actuators", J. Phys. D: Appl. Phys. 40 (2007) 605-636.

[27] F. Tochikubo, H. Arai, "Numerical simulation of streamer propagation and radical reactions in positive corona discharge in N_2/NO and N_2/O_2/NO", Jpn. J. Appl. Phys. 41 (2002) 844-852.

[28] N. L. Aleksandrov, E. M. Bazelyan, "Step propagation of a streamer in an electronegative gas", J. Exp. Theo. Phys. 91 (2000) 724-735.

[29] W. J. Yi, P. F. Williams, "Experimental study of streamers in pure N_2 and N_2/O_2 mixtures and a~13cm gap", J. Phys. D: Appl. Phys. 35 (2002) 205-218.

[30] N. L. Allen, P. N. Mikropoulos, "Dynamics of streamer propagation in air", J. Phys. D: Appl. Phys. 32 (1999) 913-919.

[31] F. Grange, N. Soulem, J. F. Loiseau, N. Spyrou, "Numerical and experimental determination of ionizing front velocity in a DC point-to-plane corona discharge", J. Phys. D. Appl. Phys. 28 (1995) 1619-1629.

[32] S. I. Yakovlenko, "The velocity of streamer propagation toward anode and cathode in He, Xe, N_2, and SF_6", Tech. Phys. Lett. 30 (2004) 354-357.

[33] S. Potamianou, N. Spyrou, J. F. Loiseau, "Numerical study of a medium pressure point-to-plane discharge", J. Phys. D: Appl. Phys. 35 (2002) 1373-1380.

[34] P. Tardiveau, E. Marode, A. Agneray, "Tracking an individual streamer branch among others in a pulsed induced discharge", J. Phys. D: Appl. Phys. 35 (2002) 2823-2829.

[35] D. Wang, M. Jikuya, S. Yoshida, T. Namihira, S. Katsuki, H. Akiyama, "Positive- and negative-pulsed streamer discharges generated by a 100-ns pulsed-power in atmospheric air", IEEE Trans. Plasma Sci. 35 (2007) 1098-1103.